ADVANCED FUNCTIONAL MATERIALS
www.afm-journal.de

Colloidal Occlusion Template Method for Micromanufacturing of Omniphobic Surfaces

Anton Grigoryev, Yuri Roiter, Ihor Tokarev, Igor Luzinov, and Sergiy Minko**

An efficient strategy to produce forests of aligned nanowires and nail-like micrometer-sized structures, whose density can be tuned in a broad range, is reported in this study. It relies on a combination of two template-assisted nanofabrication/patterning methods: electrochemical growth of metal nanowires in nanoporous sacrificial templates and partial masking of a surface with a self-assembled colloidal monolayer. A great potential of this novel approach, termed here *colloidal occlusion template method*, is demonstrated on the example of the fabrication of omniphobic surfaces comprised of nickel micronails whose density is varied to approach highest possible contact angles. After chemical modification to reduce their surface tension, these microstructures with reentrant geometry support the non-wetting Cassie state for both high-surface-tension water and low-surface-tension hexadecane. In particular, superhydrophobic behavior (contact angles exceeding 150°) is found for water, while oleophobicity (contact angles approaching 110°) is observed for hexadecane. The proposed approach can be exploited for the fabrication of a large variety of supported high-aspect-ratio nano/microstructures in applications where a surface density of features has to be several orders of magnitude lower than can be obtained with conventional template methods.

1. Introduction

Supported high-aspect-ratio micro/nanostructures made of metals, semiconductors, and conjugated polymers are generating a great deal of academic and practical interest arising from their unique properties, as well as from the promise they offer for a number of existing and emerging applications, such as ultrahigh density magnetic memory,[1] spinotronic devices and magnetic sensors,[2,3] field-emission electron emitters,[4] gas sensors,[5] biosensors,[6] electrodes for medical implants,[7] electrodes for supercapacitors and batteries,[5,8] light emitting and photovoltaic devices,[9–11] photoelectrochemical cells,[12] piezoelectric and thermoelectric energy harvesting devices,[13,14] metamaterials,[6,15] actuators,[16,17] liquid-repellent and antifouling surfaces,[18] etc. In many of these applications, control over the density of nanostructures is critical for their performance. This can be specifically illustrated with examples of nanowire-based field emitters, actuators, and liquid-repellent surfaces for which structural components have to be arranged at certain separation from each other to approach the optimal performance.

Anodized aluminum oxide (AAO) and track-etch polymer porous membranes have gained significant popularity as sacrificial templates for synthesis of conductive self-standing arrays of nanowires (and nanorods) by electrodeposition technique. Nanofabrication with these nanoporous templates offers important advantages compared to other methods, such as being simple and inexpensive, providing a great control over alignment and dimensions of nanowires, as well as the ability to generate segmented nanowires made of different materials. Commercial AAO and track-etch nanoporous filtration membranes have been a primary choice for templates in many studies due to their easy availability. However, pore densities they offer (typically ranging between 10^7 and 10^{11} pores cm^{-2}) exceed considerably densities of nanostructures desired for a number of applications. In this work we develop an approach to reduce the density of nanostructures by up to three orders of magnitude below pore densities of commonly used membrane templates. The developed approach is used here for the fabrication of a self-standing forest of nanowires and more complex overhang nail-like structures (termed hereafter *micronails*), tuning and optimization of wetting properties of the microstructures.

Wetting of solid surfaces by liquids plays a vital role in nature and technologies, as well as in materials science for analysis of surface properties of various materials.[19] There are many kinds of hydrophobic and superhydrophobic surfaces occurring naturally or created artificially.[20,21] By contrast, no oleophobic surfaces, which can repel nonpolar liquids with a low surface energy, are encountered in living systems, and a small number

A. Grigoryev, Dr. Y. Roiter, Dr. I. Tokarev, Prof. S. Minko
Department of Chemistry and Biomolecular Science
Clarkson University
8 Clarkson Avenue, Potsdam, NY 13699, USA
E-mail: itokarev@clarkson.edu; sminko@clarkson.edu
Prof. I. Luzinov
School of Materials Science and Engineering and Center for Optical Materials Science and Engineering Technologies
Clemson University
161 Sirrine Hall, Clemson, SC 29634, USA

DOI: 10.1002/adfm.201201575

of examples of corresponding synthetic oleophobic materials have been reported thus far. The materials that can efficiently repel the majority of possible liquids are referred to as *omniphobic* (i.e., phobic towards all liquids). These materials have attracted a lot of attention in recent years owing to tremendous impact they might have on industry, consumer products, and biomedical fields. Therefore, the fabrication of surfaces possessing omniphobic properties is an important direction of research.

Texturing of materials is a well-established approach to alter wettability of material's surface. A liquid in contact with such a surface is either in the Wenzel regime,[22] in which the liquid fully fills the surface irregularities, or in the Cassie regime,[23] in which the liquid shows a limited penetration into the surface irregularities, thus forming a composite interface.[24] In the latter case, the entrapped air enhances the surface hydrophobicity, resulting in very high contact angles (CAs) and low wetting hysteresis. By proper texturing, the Cassie regime can be readily achieved on low-surface-tension surfaces wetted by high-surface-tension liquids such as water. Indeed, there is a vast number of reports on so called *superhydrophobic* materials that show CAs of water exceeding 150° and low roll-off angles for water droplets. By contrast, low-surface-energy liquids, which are able to wet virtually any material with a flat surface (e.g., the maximum CA of hexadecane to be reached on a flat surface is ≈70°[25]), are unable to produce the Cassie state on commonly fabricated textured surfaces and, therefore, do not exhibit oleophobicity. Consequently, these liquids yield the completely wetted state (corresponding to the minimum of total surface energy[26]) with CAs lower than on the chemically identical flat surfaces in agreement with the Wenzel model.[22]

It has been recently demonstrated that omniphobic properties can be nevertheless obtained using specially engineered materials with topographic features having overhang or reentrant geometry.[27–36] Examples of such materials include micronail forests, micro-hoodoo arrays, woven textiles, fiber mats, and nanoparticle coatings.[27,30,31,37,38–45] The reentrant profile creates an energy barrier that preserves the liquid from the immediate irreversible transition from the Cassie state to the Wenzel state even though the latter corresponds to the minimum of surface energy of the system and the Cassie-to-Wenzel transition is favorable (for liquids with the chemical CA < 90°)[27,34,46] The energy barrier between the wetting regimes is due to capillary forces acting on the liquid-air boundary between reentrant features.[27] A reentrant profile is characterized by the texture angle ψ. In order to suspend the liquid on the reentrant surface, the chemical CA (θ) has to be greater than ψ.[34,47] Furthermore, the distance between overhang features plays an important role. In the case of micronails and micro-hoodoos, the Cassie-to-Wenzel transition occurs when the sagging liquid is able to penetrate asperities to the extent that it starts wetting an underlying support. The transition may also occur when external stimuli, such as temperature, compression, vibration, impact, or electrostatic interactions are used to overcome the aforesaid energy barrier.[48–51] The robustness of reentrant surface can be estimated for certain regular geometries using analytic models that take into account fluid properties, surface geometry, and the chemical CA.[27,31]

The common methods used to fabricate textured surfaces with reentrant geometry include photolithography and soft lithography, multistage etching, CVD, and surface structurization by irradiation with heavy ions.[52–56] However, many of the aforesaid methods are rather expensive and complicated which makes them unfeasible for the majority of research laboratories. Furthermore, photolithographic methods suffer from the diffraction resolution limit.[57] The drawbacks of soft-lithography include the lack of the possibility for scaling up and the need for replacement of stamps, which lead to a limited sample size and relatively low sample yield, respectively.[58]

The approach proposed here, which combines colloidal lithography[59] and template-assisted electrodeposition,[60] can be used to fabricate reentrant microtextures comprised of standing metal micronails at a low density. Individual micronails in this microstructure are made of nickel and comprised of high-aspect ratio wire legs and semispherical heads attached to the leg's tips. The fabrication method, termed hereafter *colloidal occlusion template method*, makes use of commercial porous anodic aluminum oxide (AAO) membranes, monodisperse polystyrene (PS) latex particles, and requires a simple electrochemical setup.

2. Results and Discussion

2.1. Colloidal Occlusion Template Method

In the experiments, we used 60-μm-thick AAO membranes as sacrificial templates for electrochemical growth of metal nanowires inside 200-nm high-aspect-ratio cylindrical pores (**Figure 1**). A membrane was covered with a conductive electrode (cathode) from one side, and an electrolyte containing Ni ions was allowed to contact with the electrode only through the membrane pores (Figure 1e). To form the caps of micronails, the electrochemical deposition was conducted long enough to completely fill the pores with nickel and continued further to allow nickel growth on the template surface (Figure 1f). As the metal reached the surface, the electrodeposition process switched from a one-dimensional (1D) mode, restricted by the walls of cylindrical pores and thereby proceeding along the pore axes, to a three-dimensional (3D) mode, restricted only by the membrane surface and hence leading to the formation of hemispherical caps. Obviously, in order to obtain isolated micronails the electrodeposition has to be stopped well before the growing neighboring caps merge.

The pore density in AAO membranes is though too high to be used for template synthesis of microtextures with omniphobic surfaces. In fact, a micronail density has to be several orders of magnitude lower than could be obtained using this kind of template. Here, we demonstrate that it is possible to reduce the density of micronails, by decreasing the amount of "working" pores available in the template membrane. To this end, we created a monolayer of PS latex particles on the membrane surface and used it as a mask to close a large fraction of the membrane's pores. The colloidal mask was prepared by a casting method, in which an alcohol dispersion of particles was spread on the surface of the AAO membrane (Figure 1b and

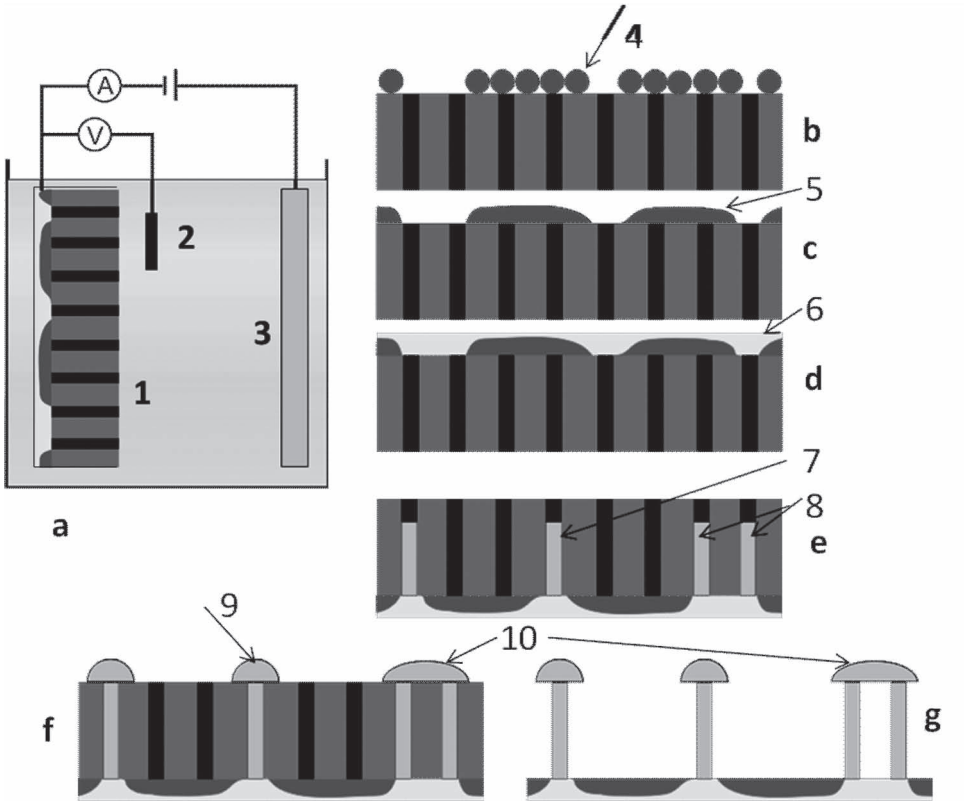

Figure 1. Schematic for the fabrication of micronails in the porous template AAO membrane with controlled density of the pores using the colloidal occlusion template method: a) electrochemical cell with the cathode, which is assembled on the porous membrane (1), reference (2), and working (3) electrodes. b–g) Schematics of the fabrication of the cathode. A fraction of AAO membrane pores is blocked by latex particles (4) that coalesce after annealing and form a latex mask (5). Gold is sputtered on the surface of the latex mask to fabricate the cathode (6). A small fraction of open pores (controlled by concentration of the latex in step (b)) is electrochemically filled with the metal and form single wires (7) and bundles of wires (8). Further deposition results in the formation of caps of the micronails (9) and merge of the wire caps of neighbor nails (10). Chemical etching of the membrane yields an array of micronails (g).

Figure 2a,i), similar to the techniques published elsewhere.[61,62] Glycerol was added to the dispersion to avoid macroscopical cracking and peeling of the colloidal mask during evaporation of alcohol. It turned out that the as-formed latex monolayer did not provide hermetic insulation of the pores causing their filling with an electrolyte solution during subsequent electrodeposition. The template membrane with pores partially blocked by latex particles yielded metal microstructures with only an incremental decrease in the density. We found, however, that the subsequent partial fusion of the latex monolayer through thermal annealing of the samples above the glass transition temperature of PS allowed us to tightly close the majority of the pores (Figure 1c). The fraction of the pores that remained open was found to depend on the concentration of latex particles in the dispersion used to create a monolayer (Figure 2a,ii). The possibility to regulate the density of available pores in the template provides the great opportunity to control the density of reentrant features and thereby to regulate the wetting properties of microtextures as demonstrated in the experiments below.

Electrochemical deposition of nickel micronails was conducted in the potentiostatic regime using a three-electrode cell and an electrolytic bath containing nickel ions (Figure 1a). The template membrane with a metal electrode deposited from the side of the PS latex mask was used as a working electrode (Figure 1d). The value of current during the electrodeposition process provided an appropriate feedback about the length of metal nanostructures being grown. In particular, as wires grew in the available pores of the template, the rate of the reduction of metal ions (and hence the current) increased due to decreasing diffusional limitations (the pores' diameter-to-length aspect ratio is 1 to 250). At the certain point, when the growing wires reached the template surface, the current exhibited a rapid increase due the sudden change in the growth regime from 1D (wires in pores) to 3D (metallic hemispheres on the template surface, Figure 1f).[63] Different diameters of nickel caps were produced by varying electrodeposition time (the current was used to monitor the cap growth).

The electrochemically grown nickel microstructures were freed from the templates by dissolution of aluminum oxide, resulting in a 2D array of standing micronails whose density matched that of the open pores of the template (Figure 1g). It has to be noted that AAO membranes are more preferable as a material of templates[64–67] than polymeric track-etch membranes which offer a similar structure of high-aspect ratio

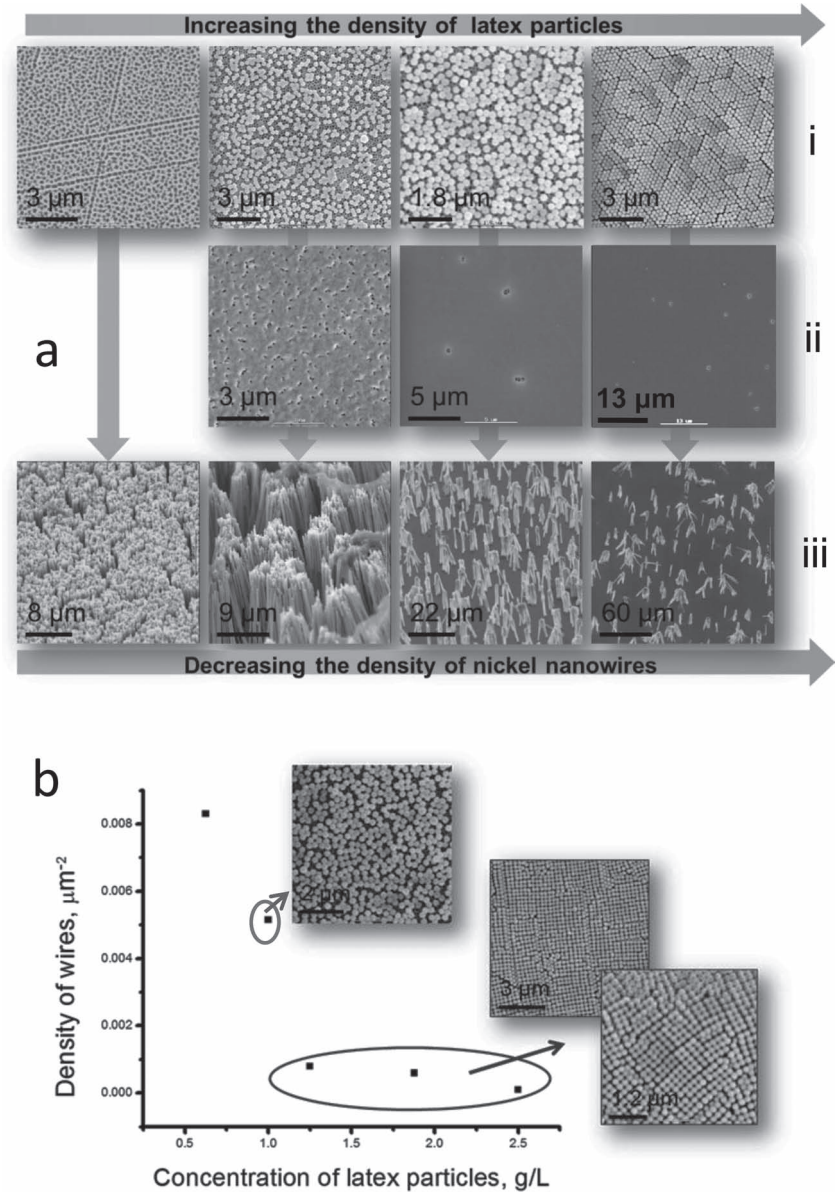

Figure 2. a) SEM images of: i) latex covered AAO membranes with an increasing density of latex particles in a monolayer; the template without particles is shown for reference (the left-most image); ii) SEM images of the latex-covered membranes after thermal annealing; partial fusion of the latex particles is observed that leads to a drastic decrease in the amount of open pores in the template; iii) SEM images of nickel nanowires grown in the corresponding templates showing an inverse correlation between the wire density and the density of latex particles. b) The density of electrodeposited nickel nanowires plotted as a function of latex particles on the template surface; the insets show SEM images of latex-covered AAO membranes used to obtain certain data points on the plot.

cylindrical pores with uniform pore diameters. First, dissolution of aluminum oxide in alkaline solutions occurs without swelling, unlike the case of dissolution of polymeric matrices in organic solvents. For instance, dissolution of polycarbonate track-etch membranes in chlorinated solvents is accompanied by initial strong swelling of the polymeric material that may cause disconnection of micronails from the conductive substrate due to strong osmotic pressure of the swelling material acting on the cap bases. Second, rigidity of AAO membranes provides an ease of handling especially after deposition of a metal electrode (metal deposition on one side of a flexible polymeric membrane causes its rolling into a tube).

The efficiency of the proposed approach in reducing the density of electrodeposited structures is demonstrated in Figure 2a,iii for the case of nickel wires (i.e., grown without caps to have unobstructed view of the structure). An inverse correlation between the density of latex particles assembled on the template surface and nickel nanowires grown on the electrode is observed (Figure 2b). The minimal wire density that can be obtained with this approach corresponds to a dense latex monolayer, forming a well-ordered 2D colloidal crystal on the template surface (the points within the circle in Figure 2b). The limitation of the method is that the allocation of open pores has random character and depends on the distribution of defects in the colloidal crystal layer.

The close examination of the fused particle monolayer shows that several pores of the AAO membrane are typically seen through open pores of the latex layer (partial dewetting of PS on alumina is a likely cause[68]). Obviously, a bundle of wires grows in this site. When micronails were grown in such templates, the caps of individual wires within a bundle were allowed to merge to form a single head. Thus, micronails comprised of ≈50 μm long multiwire legs and micrometer-sized heads were obtained after template dissolution. These high-aspect-ratio multiwire legs provided necessary support to the massive heads, ensuring the overall mechanical stability of the microtexture. Scanning electron microscopy (SEM) images of micronails show that their heads have a lateral size of 10 to 35 μm (depending on the deposition time) and consist of two opposing spherical caps (**Figure 3**c): the upper one has a hemisphere shape whereas the lower one has a much smaller curvature; the shape of the head base is likely dictated by the geometry of the AAO template.

2.2. Omniphobic Micronail Structures

The micronails were modified with a self-assembled monolayer (SAM) of perfluoroalkanethiol to reduce the surface energy of the microstructure. Figure 3a shows the data of contact angle measurements of the SAM-modified nail microstructures for two different head sizes and several nail densities. Contact angles (CAs) were probed with liquids with high

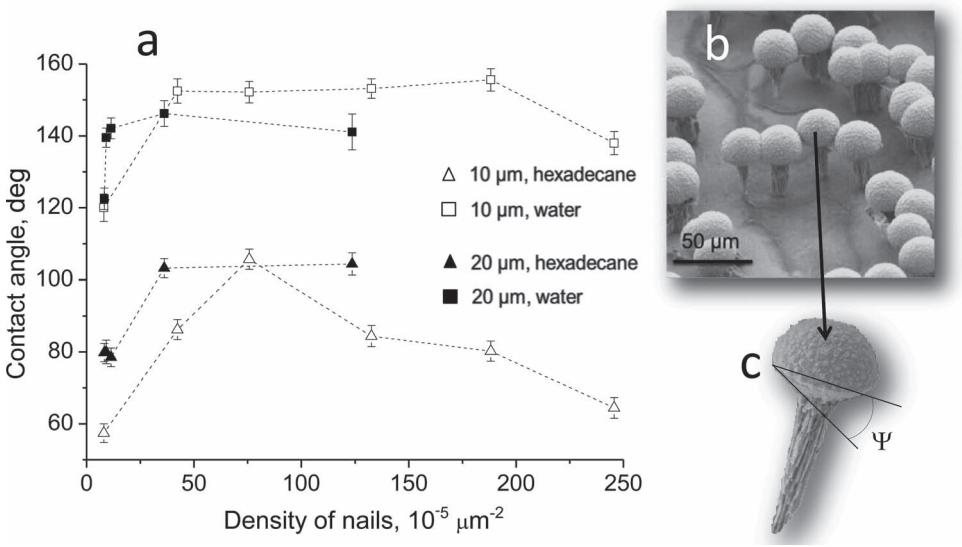

Figure 3. a) Contact angles of hexadecane and water as a function of the density of nickel micronails as measured for two diameters of heads. b) SEM image of a bed of micronails that demonstrates omniphobic properties. c) SEM image of a single micronail; the texture angle ψ of the bottom surface of the head is nonzero.

and low surface tensions, specifically water (72.8 mN/m) and hexadecane (27.47 mN/m), respectively. Windows of the optimal nail density (in terms of the highest CAs of water and hexadecane) can be identified on the plot in Figure 3a. For example, the micronails with the head size of 10 μm (**Figure 4**c) exhibit superhydrophobic properties (CAs of water exceeding 150°, Figure 4f) within a broad range of nail densities (5×10^{-4}– 2×10^{-3} μm^{-2}). The same microstructure demonstrates oleophobic properties (CAs of hexadecane exceeding 90°, Figure 4i) within a narrower window (5×10^{-4}– 1×10^{-3} μm^{-2}).

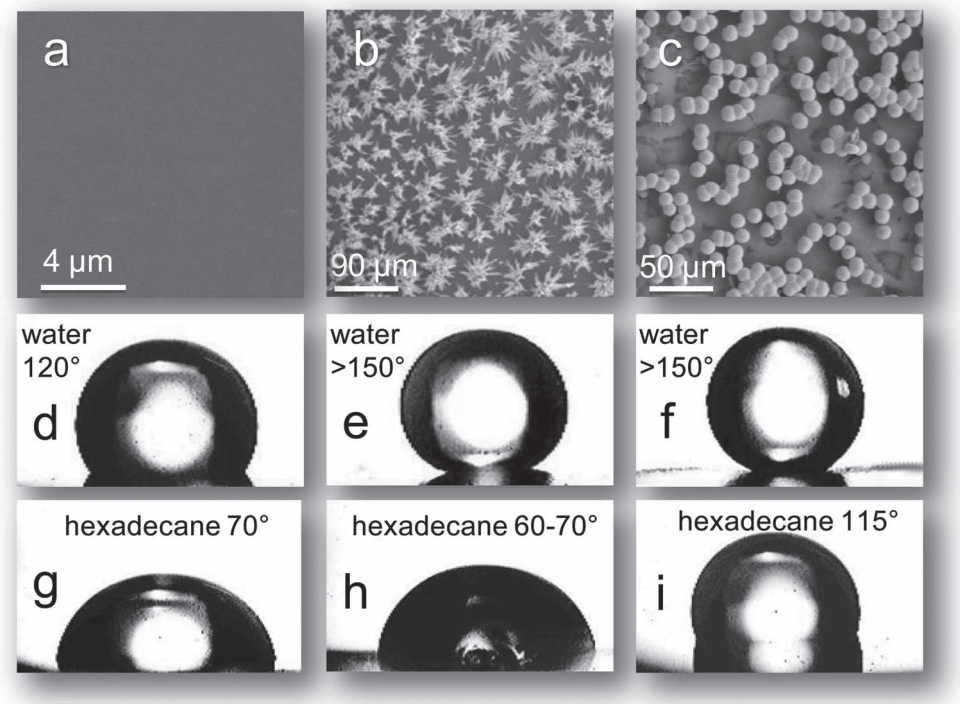

Figure 4. a–c) SEM images of the 1H,1H,2H,2H-perfluorodecanethiol functionalized samples used for contact angle measurements: a flat gold film (a), gold-coated nickel nanowires (b), and gold-coated nickel micronails (c). d–i) Contact angles of water (d–f) and hexadecane (g–i) as measured on the flat film (d, g), nanowires (e, h), and micronails (f, i).

The CA values of water and hexane on a reference flat substrate (SAM-modified gold surface, Figure 4a) are considerably lower: 120° (Figure 4d) and 70° (Figure 4g), respectively. The increased CA values of water on the SAM-modified micronails compared to the flat surface (CA > 90°) may be rationalized by both Wenzel and Cassie wetting regimes. However, the fact that the nail microstructure is more oleophobic for hexadecane (with the highest CAs of ≈105–110°) than the flat surface (CA < 90°) provides strong evidence that this low-surface-tension liquid and, thus, high-surface-tension water are in the Cassie regime at least within the above specified ranges of nail densities. (The Wenzel regime would result in a decreased CAs of hexadecane compared to the flat surface.) The composite interface (corresponding to the metastable Cassie state) is attributed to the reentrant topography of the nail microstructures which leads to upward capillary force that keeps the liquid contact line pinned to the rim of nail heads. Further evidence for the effect of the overhang geometry on wetting arises from the reference experiment in which CAs of the same liquids were measured on the surface of SAM-modified nickel nanowires (i.e., without heads, Figure 4b). Although the wire microstructure retains superhydrophobic properties for water (CAs > 150°, Figure 4e), it becomes more hydrophilic for hexadecane (CAs < 70°, Figure 4h) than the flat surface, implying that the latter liquid is in the wetting Wenzel state.

At the nail densities well below the optimal range (see the first points on the plot in Figure 3a), the microstructure does not support the composite wetting state, and the CAs of water and hexadecane are similar to those on the flat surface. The liquids at these densities sag between widely-spaced micronails to such an extent so they come into contact with the support surface. On the other hand, at the nail densities well above the optimal range, the heads merge together forming a nearly continuous surface with a high level of roughness but without overhang geometry. These microstructures are unable to form the composite interface. For example, at the nail density of 2.5×10^{-3} μm^{-2} (where the heads are merged to such an extent that they form a complete layer), the CA of hexadecane is lower and the CA of water is higher than the corresponding equilibrium CAs, demonstrating that the wetting properties are dominated by surface roughness; in particular, the roughness enhances hydrophobicity of the hydrophobic surface and oleophilicity of the oleophilic one according to the Wenzel model.

As already mentioned, the highest CAs for hexadecane achieved in our experiments were about 105°–110° (Figure 3a). These CA values are lower than those reported for periodic micro-hoodoo arrays,[27,31,69] for which superomniphobic properties (CAs above 150° for both water and oils) have been observed. The discrepancy in the performance of micronails and micro-hoodoos lies primarily in the spatial arrangement of overhang structures. Specifically, careful examination of the SEM images reveals that the majority of micronails are congregated within clusters (where micronails are in contact with each other; see Figure 3b). The average distance between the clusters is obviously much higher than in a periodic lattice or a random structure of the same density but comprised of isolated micronails. Micronail clustering makes possible the situation in which a microstructure consisting of isolated overhang features supports the Cassie regime, whereas a clustered microstructure of the same density of features, exhibiting relatively large voids between the clusters, does not. To achieve the composite interface in the latter case, the density of features has to be increased to the level when the liquid sagging in voids between clusters does not wet the supporting substrate. An increased density translates in turn into a higher fraction of the material's surface in contact with the liquid (f_s) and to lower apparent contact angles according to the Cassie equation. For the studied microstructure and hexadecane as the testing liquid, the Cassie state is reached when f_s approaches 0.4. The high value of f_s leads to the observed CAs of hexadecane.

The nonzero texture angle ψ does not affect the apparent contact angle but the stability of the composite interface. Its value at the head's rim (ca. 30°), however, is much smaller than chemical CA of hexadecane on fluorinated surface (70°), and hence its impact on robustness of the Cassie regime is small.

3. Conclusions

A novel colloidal occlusion template method has been demonstrated. This facile and inexpensive method, which combines colloidal masking and template-assisted electrochemical deposition, was used to generate omniphobic surfaces comprised of nail-shaped reentrant features on solid substrates. After chemical modification to reduce the surface tension, these forests of micronails exhibited both superhydrophobicity and oleophobicity. The unique properties of the obtained microtextures open a number of new prospective applications, whose investigation is under way in our laboratory.

4. Experimental Section

Commercial porous AAO membranes (Anodisc, from Whatman, Inc., UK) having the diameter of 13 mm, the nominal pore size of 200 nm, and the pore density ≈10^{13} m^{-2} were used as sacrificial templates. A dispersion of sulfonated PS latex (Interfacial Dynamics Corp., OR) with the average particle size of 200 nm and a low polydispersity was used for the preparation of colloidal masks on the membrane surface. To this end, 70 μL of a latex dispersion in ethanol, which contained from 1 to 2.5 g/L of PS particles and 2 vol% of glycerol, was uniformly cast on one side of the membrane and dried. After the complete evaporation of ethanol, the sample was held in vacuum oven (140 °C and ca. 2×10^3 Pa) for 20 min to fuse the PS particles and form a porous mask that adheres well to the membrane surface and hermetically seals the membrane pores under the mask. Then, a 1-μm-thick gold (99.99%) layer was sputtered (using CrC-150 Sputtering System, Torr International, NY) on the latex side of the template to serve as an electrode during electrodeposition. The template with the gold electrode was placed on a glass support with the gold side facing the glass. Electrode connections were made with silver paint, and the sample's perimeter was insulated with a 20 wt% PMMA solution in a solvent mixture of methyl ethyl ketone and ethyl acetate (7:3 v/v). As the PMMA insulator dried, electrochemical deposition was performed through the uncovered central part of the template at potentiostatic mode (–1 V vs Ag/AgCl) in the electrochemical bath containing 300 g/L of $NiSO_4 \cdot 6H_2O$, 45 g/L of $NiCl_2 \cdot 6H_2O$, saturated H_3BO_3 (45 g/L) at pH 3.3 at room temperature. The sample was the cathode whereas a nickel plate served as the anode. After the electrochemical deposition of nickel, the sample was rinsed with deionized water. Then, the AAO membrane was dissolved in 1.5 M NaOH for 30 min while steering to expose the nickel microstructure and washed thoroughly in deionized water. The substrates with the nickel microstructures were sputter-coated with

a 200-to-500-nm-thick gold layer, then thiolized in a 0.01 mM hexane solution of 1H,1H,2H,2H-perfluorodecanethiol (Sigma-Aldrich, MO) for 22 h to reduce the surface tension of the nickel surface. Contact angle measurements were conducted using a self-made contact angle goniometer. SEM images were acquired using a JSM 6300 instrument (15 kV, JEOL Ltd., Japan).

Acknowledgements

The authors acknowledge the support of NSF via CMMI grants 0825832 and 0825773.

Received: June 12, 2012
Published online: September 25, 2012

[1] X. M. Kou, X. Fan, R. K. Dumas, Q. Lu, Y. P. Zhang, H. Zhu, X. K. Zhang, K. Liu, J. Q. Xiao, *Adv. Mater.* **2011**, *23*, 1393–1397.
[2] X. B. Huang, L. W. Tan, H. Cho, B. J. H. Stadler, *J. Appl. Phys.* **2009**, *105*.
[3] A. Mourachkine, O. V. Yazyev, C. Ducati, J. P. Ansermet, *Nano Lett.* **2008**, *8*, 3683–3687.
[4] L. Vila, P. Vincent, L. Dauginet-De Pra, G. Pirio, E. Minoux, L. Gangloff, S. Demoustier-Champagne, N. Sarazin, E. Ferain, R. Legras, L. Piraux, P. Legagneux, *Nano Lett.* **2004**, *4*, 521–524.
[5] J. Chen, L. N. Xu, W. Y. Li, X. L. Gou, *Adv. Mater.* **2005**, *17*, 582–586.
[6] A. V. Kabashin, P. Evans, S. Pastkovsky, W. Hendren, G. A. Wurtz, R. Atkinson, R. Pollard, V. A. Podolskiy, A. V. Zayats, *Nat. Mater.* **2009**, *8*, 867–871.
[7] S. Matefi-Tempfli, M. Matefi-Tempfli, *Adv. Mater.* **2009**, *21*, 4005–4010.
[8] Y. Cao, T. E. Mallouk, *Chem. Mater.* **2008**, *20*, 5260–5265.
[9] R. Yan, D. Gargas, P. Yang, *Nat. Photonics* **2009**, *3*, 569–576.
[10] J. R. Morber, X. D. Wang, J. Liu, R. L. Snyder, Z. L. Wang, *Adv. Mater.* **2009**, *21*, 2072–2076.
[11] M. Law, L. E. Greene, J. C. Johnson, R. Saykally, P. Yang, *Nat. Mater.* **2005**, *4*, 455–459.
[12] R. van de Krol, Y. Liang, J. Schoonman, *J. Mater. Chem.* **2008**, *18*, 2311–2320.
[13] A. I. Hochbaum, R. Chen, R. D. Delgado, W. Liang, E. C. Garnett, M. Najarian, A. Majumdar, P. Yang, *Nature* **2008**, *451*, 163–167.
[14] S. Xu, Y. Qin, C. Xu, Y. G. Wei, R. S. Yang, Z. L. Wang, *Nat. Nanotechnol.* **2010**, *5*, 366–373.
[15] J. Yao, Z. W. Liu, Y. M. Liu, Y. Wang, C. Sun, G. Bartal, A. M. Stacy, X. Zhang, *Science* **2008**, *321*, 930–930.
[16] Y. Berdichevsky, Y. H. Lo, *Adv. Mater.* **2006**, *18*, 122–125.
[17] X. M. He, C. Li, F. G. Chen, G. Q. Shi, *Adv. Funct. Mater.* **2007**, *17*, 2911–2917.
[18] K. M. Ainslie, G. Sharma, M. A. Dyer, C. A. Grimes, M. V. Pishko, *Nano Lett.* **2005**, *5*, 1852–1856.
[19] D. Y. Kwok, A. W. Neumann, *Adv. Colloid Interface Sci.* **1999**, *81*, 167–249.
[20] M. Motornov, R. Sheparovych, R. Lupitskyy, E. McWilliams, S. Minko, *Adv. Mater.* **2008**, *20*, 200–205.
[21] M. J. Xu, N. Lu, H. B. Xu, D. P. Qi, Y. D. Wang, S. L. Shi, L. F. Chi, *Soft Matter* **2010**, *6*, 1438–1443.
[22] R. N. Wenzel, *Ind. Eng. Chem.* **1936**, *28*, 988.
[23] A. B. D. Cassie, S. Baxter, *Trans. Faraday Soc.* **1944**, *40*, 546–551.
[24] G. Whyman, E. Bormashenko, T. Stein, *Chem. Phys. Lett.* **2008**, *450*, 355–359.
[25] N. V. Venkataraman, S. Zurcher, A. Rossi, S. Lee, N. Naujoks, N. D. Spencer, *J. Phys. Chem. C* **2009**, *113*, 5620–5628.
[26] D. Quere, *Annu. Rev. Mater. Res.* **2008**, *38*, 71–99.
[27] A. Tuteja, W. J. Choi, G. H. McKinley, R. E. Cohen, M. F. Rubner, *MRS Bull.* **2008**, *33*, 752–758.
[28] N. A. Patankar, *Langmuir* **2004**, *20*, 8209–8213.
[29] A. Marmur, *Langmuir* **2008**, *24*, 7573–7579.
[30] A. Ahuja, J. A. Taylor, V. Lifton, A. A. Sidorenko, T. R. Salamon, E. J. Lobaton, P. Kolodner, T. N. Krupenkin, *Langmuir* **2008**, *24*, 9–14.
[31] A. Tuteja, W. Choi, M. L. Ma, J. M. Mabry, S. A. Mazzella, G. C. Rutledge, G. H. McKinley, R. E. Cohen, *Science* **2007**, *318*, 1618–1622.
[32] D. W. Han, A. J. Steckl, *Langmuir* **2009**, *25*, 9454–9462.
[33] L. Joly, T. Biben, *Soft Matter* **2009**, *5*, 2549–2557.
[34] M. Nosonovsky, *Langmuir* **2007**, *23*, 3157–3161.
[35] L. L. Cao, H. H. Hu, D. Gao, *Langmuir* **2007**, *23*, 4310–4314.
[36] S. Herminghaus, *Europhys. Lett.* **2000**, *52*, 165–170.
[37] A. Grigoryev, I. Tokarev, K. G. Kornev, I. Luzinov, S. Minko, *J. Am. Chem. Soc.* **2012**, *134*, 12916–12919.
[38] A. Tuteja, W. Choi, J. M. Mabry, G. H. McKinley, R. E. Cohen, *Proc. Natl. Acad. Sci. USA* **2008**, *105*, 18200–18205.
[39] W. Choi, A. Tuteja, S. Chhatre, J. M. Mabry, R. E. Cohen, G. H. McKinley, *Adv. Mater.* **2009**, *21*, 2190–2195.
[40] S. S. Chhatre, W. Choi, A. Tuteja, K. C. Park, J. M. Mabry, G. H. McKinley, R. E. Cohen, *Langmuir* **2010**, *26*, 4027–4035.
[41] T. Darmanin, F. Guittard, S. Amigoni, E. T. de Givenchy, X. Noblin, R. Kofman, F. Celestini, *Soft Matter* **2011**, *7*, 1053–1057.
[42] T. Fujii, Y. Aoki, H. Habazaki, *Langmuir* **2011**, *27*, 11752–11756.
[43] C. T. Hsieh, F. L. Wu, W. Y. Chen, *Mater. Chem. Phys.* **2010**, *121*, 14–21.
[44] J. P. Zhang, S. Seeger, *Angew. Chem. Int. Ed.* **2011**, *50*, 6652–6656.
[45] A. Steele, I. Bayer, E. Loth, *Nano Lett.* **2009**, *9*, 501–505.
[46] A. Marmur, *Langmuir* **2003**, *19*, 8343–8348.
[47] D. Quere, *Rep. Prog. Phys.* **2005**, *68*, 2495–2532.
[48] A. Lafuma, D. Quere, *Nat. Mater.* **2003**, *2*, 457–460.
[49] G. Londe, A. Chunder, L. Zhai, H. J. Cho, *Appl. Phys. Lett.* **2009**, *94*, 164104.
[50] E. Bormashenko, R. Pogreb, G. Whyman, Y. Bormashenko, M. Erlich, *Appl. Phys. Lett.* **2007**, *90*, 201917.
[51] M. Im, H. Im, J. H. Lee, J. B. Yoon, Y. K. Choi, *Soft Matter* **2010**, *6*, 1401–1404.
[52] Z. J. Han, B. Tay, C. M. Tan, M. Shakerzadeh, K. Ostrikov, *ACS Nano* **2009**, *3*, 3031–3036.
[53] R. T. R. Kumar, K. B. Mogensen, P. Boggild, *J. Phys. Chem. C* **2010**, *114*, 2936–2940.
[54] Z. J. Han, B. K. Tay, M. Shakerzadeh, K. Ostrikov, *Appl. Phys. Lett.* **2009**, *94*, 223106.
[55] G. P. Li, T. Chen, B. Yan, Y. Ma, Z. Zhang, T. Yu, Z. X. Shen, H. Y. Chen, T. Wu, *Appl. Phys. Lett.* **2008**, *92*, 173104.
[56] S. M. M. Ramos, A. Benyagoub, B. Canut, C. Jamois, *Langmuir* **2009**, *26*, 5141–5146.
[57] G. M. Wallraff, W. D. Hinsberg, *Chem. Rev.* **1999**, *99*, 1801–1821.
[58] Y. N. Xia, G. M. Whitesides, *Annu. Rev. Mater. Sci.* **1998**, *28*, 153–184.
[59] S. M. Yang, S. G. Jang, D. G. Choi, S. Kim, H. K. Yu, *Small* **2006**, *2*, 458–475.
[60] C. R. Martin, *Science* **1994**, *266*, 1961–1966.
[61] S. Maenosono, C. D. Dushkin, Y. Yamaguchi, K. Nagayama, Y. Tsuji, *Colloid Polym. Sci.* **1999**, *277*, 1152–1161.
[62] G. S. Lazarov, N. D. Denkov, O. D. Velev, P. A. Kralchevsky, K. Nagayama, *J. Chem. Soc., Faraday Trans.* **1994**, *90*, 2077–2083.
[63] M. E. Toimil-Molares, V. Buschmann, D. Dobrev, R. Neumann, R. Scholz, I. U. Schuchert, J. Vetter, *Adv. Mater.* **2001**, *13*, 62–65.

[64] A. P. Li, F. Muller, A. Birner, K. Nielsch, U. Gosele, *J. Appl. Phys.* **1998**, *84*, 6023–6026.
[65] J. P. O'Sullivan, G. C. Wood, *Proc. R. Soc. London, Ser. A* **1970**, *317*, 511–543.
[66] W. Lee, K. Nielsch, U. Gosele, *Nanotechnology* **2007**, *18*, 475713.
[67] W. Lee, K. Schwirn, M. Steinhart, E. Pippel, R. Scholz, U. Gosele, *Nat. Nanotechnol.* **2008**, *3*, 234–239.
[68] T. Ondarcuhu, A. Piednoir, *Nano Lett.* **2005**, *5*, 1744–1750.
[69] A. Tuteja, W. Choi, J. M. Mabry, G. H. McKinley, R. E. Cohen, *Proc. Natl. Acad. Sci. USA* **2008**, *105*, 18200–18205.